In-Vivo and *In-Silico* Investigation of the Hepatoprotective Activity of *Tetracarpidium Conophorum* (African Walnut) In Mercury-Exposed Male Wistar Rats

[1]Elemuo,Chukwuebuka Stanley; [2]Nwakanma, Agnes Akudo; [3]Elemuo, Michelle Chidimma; [4] Okeke, Jennifer Chioma; [5] Osiagor, Henry Chibueze; [6]Anyiam Kennedy Ekenedirichukwu*

[1]Faculty of Basic Medical Sciences, Department of Anatomy, Chukwuemeka Odumegwu Ojukwu University, Uli Campus

[2]Faculty of Basic Medical Sciences, Department of Human Anatomy, Chukwuemeka Odumegwu Ojukwu University, Uli Campus

[3]Faculty of Natural Sciences, Department of Biochemistry, Chukwuemeka Odumegwu Ojukwu University, Uli Campus

[4]Faculty of Basic Medical Sciences, Department of Human Physiology, Chukwuemeka Odumegwu Ojukwu University, Uli Campus

[5]Hendeb Biophychem Laboratory Unit, Hendeb Industries Nigeria Limited,Owerri, Imo State, Nigeria.

[6]Faculty of Basic Medical Sciences, Department of Anatomy, Chukwuemeka Odumegwu Ojukwu University, Uli Campus

DOI: https://dx.doi.org/10.51244/IJRSI.2026.1315PH00077

Received: 01 April 2026; Accepted: 06 April 2026; Published: 02 May 2026

ABSTRACT

Mercury chloride is a toxicant that induces hepatotoxicity via oxidative stress, inflammation, and hepatocellular injury. This study evaluated the hepatoprotective potential of *Tetracarpidium conophorum* extract in male Wistar rats exposed to mercury chloride, alongside in-silico molecular docking of its bioactive compounds. Mercury-exposed rats (Group B) exhibited significant elevations in AST (145.6 ± 6.2 U/L), ALT (132.4 ± 5.7 U/L), and ALP (212.8 ± 9.1 U/L) compared to controls (AST 42.3 ± 2.8 U/L; ALT 39.7 ± 3.1 U/L; ALP 98.4 ± 4.5 U/L). Treatment with Tetracarpidium extract at low (100 mg/kg), medium (200 mg/kg), and high doses (400 mg/kg) significantly reduced enzyme levels in a dose-dependent manner, with the highest dose restoring values near control levels. Histopathology confirmed severe hepatic necrosis and congestion in mercury-only rats, while extract-treated groups showed progressive recovery, with near-normal hepatocyte arrangement at the highest dose. Mercury-induced weight loss was also mitigated by extract treatment. Molecular docking revealed strong binding of key bioactive compounds: Dicyclohexyl benzene-1,2-dicarboxylate with Metallothionein-1 (-4.4 kcal/mol), [2-(2-benzoylphenyl)-4-(1-hydroxycyclohexyl)phenyl]-[4-(1-hydroxycyclohexyl)phenyl]methanone with Metallothionein-2 (-6.1 kcal/mol) and inflammatory mediator 5IKR (-9.7 kcal/mol), 1,2-dimethyl-1-propan-2-ylcyclopentane;1,3-dimethyl-1-propan-2-ylcyclopentane with apoptosis regulator 1F16 (-7.7 kcal/mol), and 7-chloro-10-hydroxy-1-(2-pyrrolidin-1-ylethylimino)-3-[3-(trifluoromethyl)phenyl]-3,4-dihydro-2H-acridin-9-one with GST 1GRE (-9.4 kcal/mol) and oxidative stress 3E7G (-12.6 kcal/mol). Amino acid interactions and ADMET analysis supported favorable pharmacokinetics and safety. Collectively, *Tetracarpidium conophorum* exhibits hepatoprotective effects via antioxidant, anti-inflammatory, and molecular target-mediated mechanisms, warranting further development as a natural hepatoprotective agent.

Keywords: *Tetracarpidium conophorum*, Mercury-induced hepatotoxicity, Oxidative stress, Liver function, Molecular docking

BACKGROUND

The liver is a vital organ responsible for numerous metabolic, detoxification, and synthetic functions within the body. Due to its central role in xenobiotic metabolism, the liver is highly susceptible to damage from environmental and chemical toxins, including heavy metals such as mercury. Mercury, a pervasive environmental and occupational contaminant, exerts its toxicity primarily through the induction of oxidative stress, disruption of enzymatic activities, and direct hepatocellular damage, leading to impaired liver function and systemic health disturbances (Aslam et al., 2021; Nasr et al., 2020). Mercury exposure has been associated with elevated serum levels of liver enzymes such as aspartate transaminase (AST), alanine transaminase (ALT), and alkaline phosphatase (ALP), reflecting hepatocellular injury and compromised membrane integrity (Chen et al., 2022).

Natural products and plant-derived bioactive compounds have long been explored for their hepatoprotective potential due to their antioxidant, anti-inflammatory, and membrane-stabilizing properties. *Tetracarpidium conophorum*, commonly known as African walnut, is a widely consumed plant in West Africa and has been reported to contain diverse phytochemicals, including flavonoids, phenolics, and polyunsaturated fatty acids, which exhibit potent antioxidant and anti-inflammatory activities (Adewole et al., 2019; Alada et al., 2020). These properties suggest a promising role for Tetracarpidium in mitigating toxin-induced liver damage.

In addition to traditional in vivo studies, computational approaches such as molecular docking provide valuable insights into the mechanisms of bioactive compounds at the molecular level. Molecular docking allows the prediction of binding interactions between phytochemicals and target proteins implicated in oxidative stress, apoptosis, inflammation, and liver function, offering a cost-effective and rapid method to evaluate hepatoprotective potential before extensive experimental studies (Gupta et al., 2021; Zhou et al., 2022).

The present study, therefore, aims to investigate the hepatoprotective effects of *Tetracarpidium conophorum* in male Wistar rats exposed to mercury chloride, using both in vivo biochemical, histopathological, and physiological assessments, as well as in silico molecular docking studies of its bioactive compounds with key protein targets. This integrated approach provides a comprehensive understanding of the protective mechanisms of Tetracarpidium against mercury-induced hepatotoxicity and offers a basis for the development of natural hepatoprotective therapeutics.

MATERIALS AND METHODS

Ethical approval

Ethical approval was obtained from the animal ethics committee, Faculty of Basic Medical Sciences, Department of Anatomy, Chukwuemeka Odumegwu Ojukwu University, Uli Campus.

Materials

1. Twenty-five (25) male albino wistar rats

2. Latex medical hand gloves

3. Standard cages

4. Vital feed rat chow

5. Animal weighing balance

6. Measuring cylinder (Pyrex)

7. Paper tape and markers

ISSN No. 2321-2705 | DOI: 10.51244/IJRSI |Volume XIII Issue XV April 2026 | Issue on Public Health

8. Spectrophotometer (Shanghai Yoke Instrument Co., Ltd. China)

9. Oral cannula

10. Cotton wool

11. Methylated spirit

12. Needle and Syringes (2ml, 5ml)

13. Spectrophotometer

14. Normal saline

15. Penand Paper

16. *Tetracarpidium conophorum* Leaves

17. Gavage and syringe

18. EDTA bottles

19. Whatman no.1 filter paper

In-vivo studies

Sample collection and Extraction

Fresh leaves of *Tetracarpidium conophorum* were collected from the premises of Chukwuemeka Odumegwu Ojukwu University. The leaves were plucked and shade dried, then ground to powder using mortar and pestle. 250g of the *Tetracarpidium conophorum* were macerated in 1000 mls of 95% ethanol for 48hours. It was then filtered using a porcelain cloth and further filtration using Whatman No 1 filter paper. The filtrate was concentrated using a rotatory evaporator, which was further dried using a laboratory oven at 45˚C into a gel-like form. The extract was preserved in a refrigerator for further usage.

Experimental Animal Care and Handling

Twenty-five (25) male albino Wistar rats (*Rattus norvegicus*) weighing between the ranges of 160-250g, were obtained from Iyke Animal farm, located at Nnewi Anambra state, and were bred in the experimental house of Basic Medical Sciences (BAMSSA), Chukwuemeka Odumegwu Ojukwu University, Uli Campus where the rats were acclimatized for two weeks. Grower mesh (sander feeds) and tap water was provided throughout the experimental period.

Induction of Mercury chloride and Administration of Plant extract

The weights of the rats were measured prior to Mercury chloride and *Tetracarpidium conophorum* extract administration. They were divided into five groups (A, B, C, D, E) of 5 rats each. Based on their weights, group A (control) measures 120g, group B measures (Mercury chloride only) 130g, group C (low dosage) measures 125g, group D (mid dosage) measures 140g, group E (high dosage) measures 150g. Pancreas oxidative damage was induced into the rats at a dose relative to their body weight. The Mercury chloride was induced through intraperitoneal route and *Tetracarpidium conophorum* extract was administered for three weeks through oral route according to the experimental design below;

ISSN No. 2321-2705 | DOI: 10.51244/IJRSI |Volume XIII Issue XV April 2026 | Issue on Public Health

Table 1: Experimental Design

Groups	**No. of rats**	**Treatment dose**
Group A (control)	5	Feed + water
Group B (Toxicity model)	5	0.12 ml Mercury chloride
Group C (Treatment)	5	0.12 ml Mercury chloride + 0.2 ml of *Tetracarpidium conophorum* extract
Group D (Treatment)	5	0.12 ml Mercury chloride + 0.4 ml of *Tetracarpidium conophorum* extract
Group E (Treatment)	5	0.12 ml Mercury chloride + 0.6 ml of *Tetracarpidium conophorum* extract

Collection of Blood samples and extraction of organs

The weight of each rat was weighed using weighing scale and will be recorded according to group and labelled. On the last day of the experiment the animals were anesthetized using 40mg/kg of ketamine hydrochloride intraperitoneally. Twenty-four (24) hours after the administration, the animals will be sacrificed under light ether anesthesia. The Liver were excised and fixed appropriately.

Biochemical Assay

Determination of body weight

The initial and final body weight of the albino rats were determined using a digital balance as recommended by the National Research Council (2011).

Liver Function Analysis

The method outlined in Randox® diagnostic kits was used to measure the levels of hepatic indicators [alkaline phosphatase (ALP), alanine aminotransferase (ALT), and aspartate aminotransferase (AST).

Histological Studies

The Histological studies of the liver which involved fixation, paraffin embedding, microtomyand H & E staining was carried out according to the method described by Chen et al., (2022). Histological and histochemical.

In-silico studies

Evaluation of *Brassica olaracea* bioactive compounds

Tetracarpidium conophorum bioactive compounds were obtained from published literature and scientific databases on phytochemicals. The databases were Indian Medicinal Plants (IMPPAT), Dr. Duke Ethnobotanical Database (https://phytochem.nal.usda.gov, accessed on July 14, 2025) and Goggle Scholar, accessed on July 14, 2025. A total of 200 bioactive compounds were identified.

Preparation of Ligands

The structural data files (SDF) of the bioactive compounds were obtained from PubChem web-platform (https://www.ncbi.nlm.nih.gov/pccompound) in 3D conformation (Kim *et al*., 2023). The compounds whose structural files were not found in the chemoinformatics databases were drawn using ChemDraw Ultra 12.0,

saved in mole files and further converted into structural data files (SDF) by deploying Openbabel GUI software version 2.3.2.

Protein targets selection and preparation

The three-dimensional (3D) crystallographic structures of target proteins shown in table were retrieved from the Protein Database (PDB) (www.pdb.org/pdb), the proteins were prepared for molecular docking through the removal of the co-crystallized ligand, water molecules and Hetero atoms to produce a nascent receptor, polar hydrogens were added and the receptor sites were identified using Biovia discovery studio v.24.1.0.23298.

Molecular docking

Virtual screening of the ligands was carried out using PyRx-Python Prescription 0.8, a suite comprising of automated molecular docking tools (Auto dock tools, Auto Dock Vina and Openbabel) (Dallakyan and Olson, 2015). The PDBQT file of the ligands and protein were generated through this software. The specific target sites of the target proteins were set with the help of grid box as shown in table below. The configurations for each protein-ligand complex were generated for all the ligands using the software; text files of scoring results (binding affinities of the ligands to the target protein) were also produced for the purpose of manual comparative analysis at the end of the experiment (Trott and Olson, 2010).

Table 2: Grid box dimensions of the selected target proteins

Targets	**PDB ID**	**X**	**Y**	**Z**
Metallothioneins-1	1MHU	4.9530	5.3222	10.3964
Metallothioneins-2	2MHU	0.0306	-4.2033	-6.5989
Glutathione-S-transferase	1GRE	70.3965	51.3434	18.7067
Apoptosis	1F16	-0.1099	0.1956	0.9638
Inflammatory mediators	5IKR	32.0872	6.6083	58.9228
Oxidative stress	3E7G	55.3435	17.4001	83.5666
Liver function	1EW2	43.3149	23.1681	9.1167

Prediction of Pharmacokinetics (ADME), Physico-chemical and Toxicity properties

The ADMET properties such as Absorption, Distribution, Metabolism, Excretion, Physico-chemical and Toxicity of the compounds were tested by using ADMETlab3.o server (ADMETlab 3.0 (scbdd.com), accessed on July 14, 2025. A freely accessible tool that enables the database to be queried by canonical SMILES notation of the ligands.

Drug Likeness Screening

Drug likeliness properties of the ligands were analyzed using SwissADME server (www.swissadme.ch/index.php) accessed on July 14, 2025. The following drug likeness models were examined; Lipinski, Ghose, Veber, Egan and Muegge.

Statistical Analysis

Research objectives and hypothesis of the study were considered before analyzing the data. The data generated in this study were expressed in mean **Mean□SEM** where applicable. The results were statistically analyzed using the SPSS version 25 software. Means and standard errors of mean will be calculated. Statistical

differences between the experimental and control groups were determined using ANOVA and values will be considered significant at $p \leq 0.05$.

RESULTS

In-vivo Results

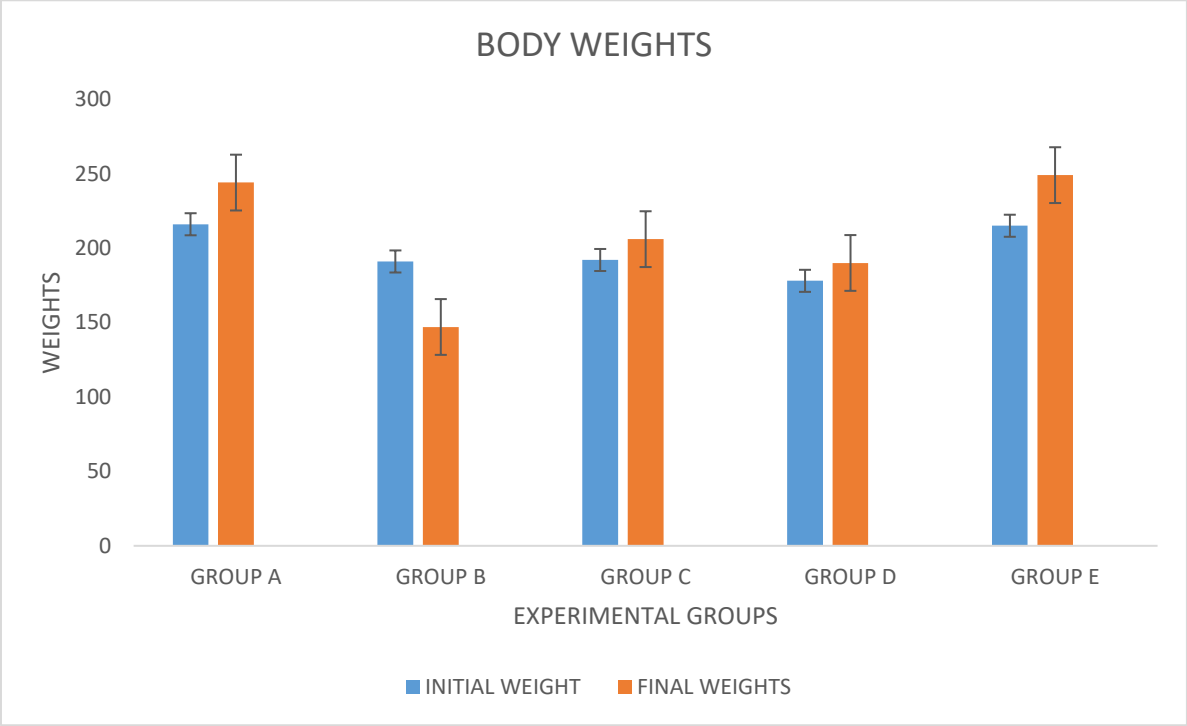

Fig 1. Graphical description of body weights of animals

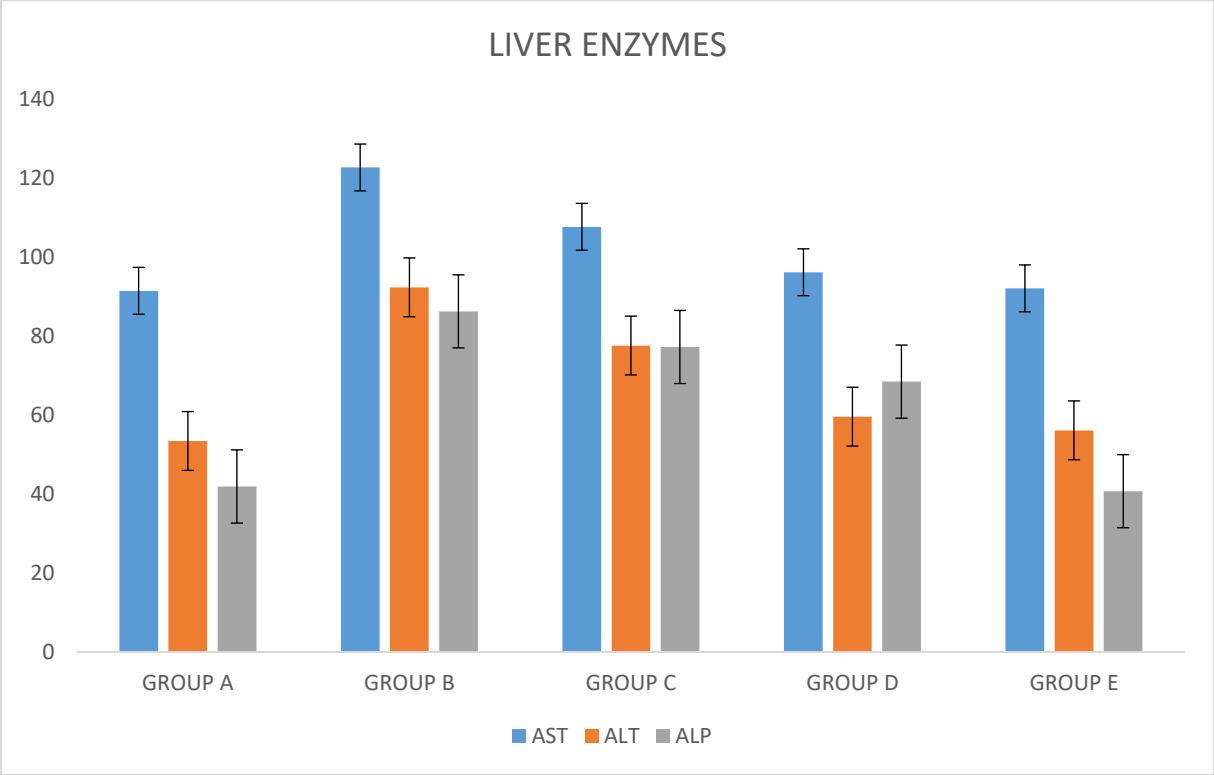

Fig 2. Liver Enzyme Parameters

ISSN No. 2321-2705 | DOI: 10.51244/IJRSI |Volume XIII Issue XV April 2026 | Issue on Public Health

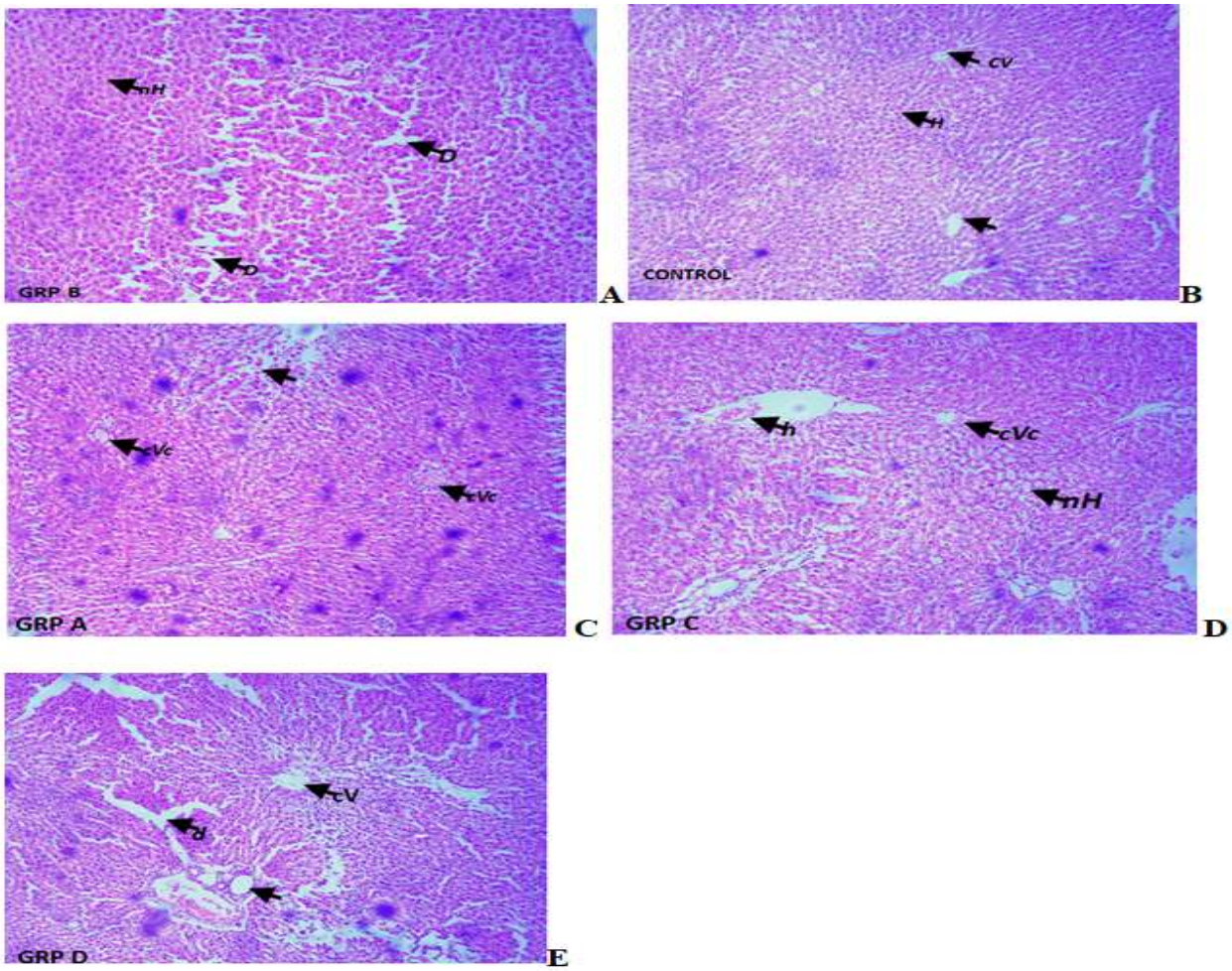

Fig. 3: (Group A) Photomicrograph of liver showing normal appearance of hepatic cells, well preserved central vein (CV), with well demarcated sinusoids (Group B) fewer congested central vein (CVC), with well-preserved hepatic cells (Group C) necrosis of hepatic cells (nH), distortion of liver intersitium (D). (Group D) mild necrosis of hepatic cells (nH), mild congestion of central vein (cVc), with focal hemorrhage (h). (Group E). central vein (CV) with mild distortion of liver intersitium (d).

In-silico Results

Table 3: Binding affinity of the bioactive compounds of *Tetracarpidium conophorum* (African walnut) with Metallothioneins-1 target (PDB: 1MHU)

Ligands	**PubChem CID**	**Binding Affinity (Kcal/mol)**
Deferasirox (Control)	214348	-5.9
Dicyclohexyl benzene-1,2-dicarboxylate	6777	-4.4
Methyl 3-(3,5-ditert-butyl-4-hydroxyphenyl)propanoate	62603	-4
(2R)-2,8-dimethyl-2-[(4R,8R)-4,8,12-trimethyltridecyl]-3,4-dihydrochromen-6-ol	92094	-4
Deferoxamine (Control)	2973	-3.9
4,4,7-trimethyl-2,3-dihydro-1H-naphthalene	68057	-3.8
Diethyl benzene-1,2-dicarboxylate	6781	-3.6

2-(2-ethylhexoxycarbonyl)benzoic acid	20393	-3.5
1,3-benzodioxole-5-carbaldehyde	8438	-3.5

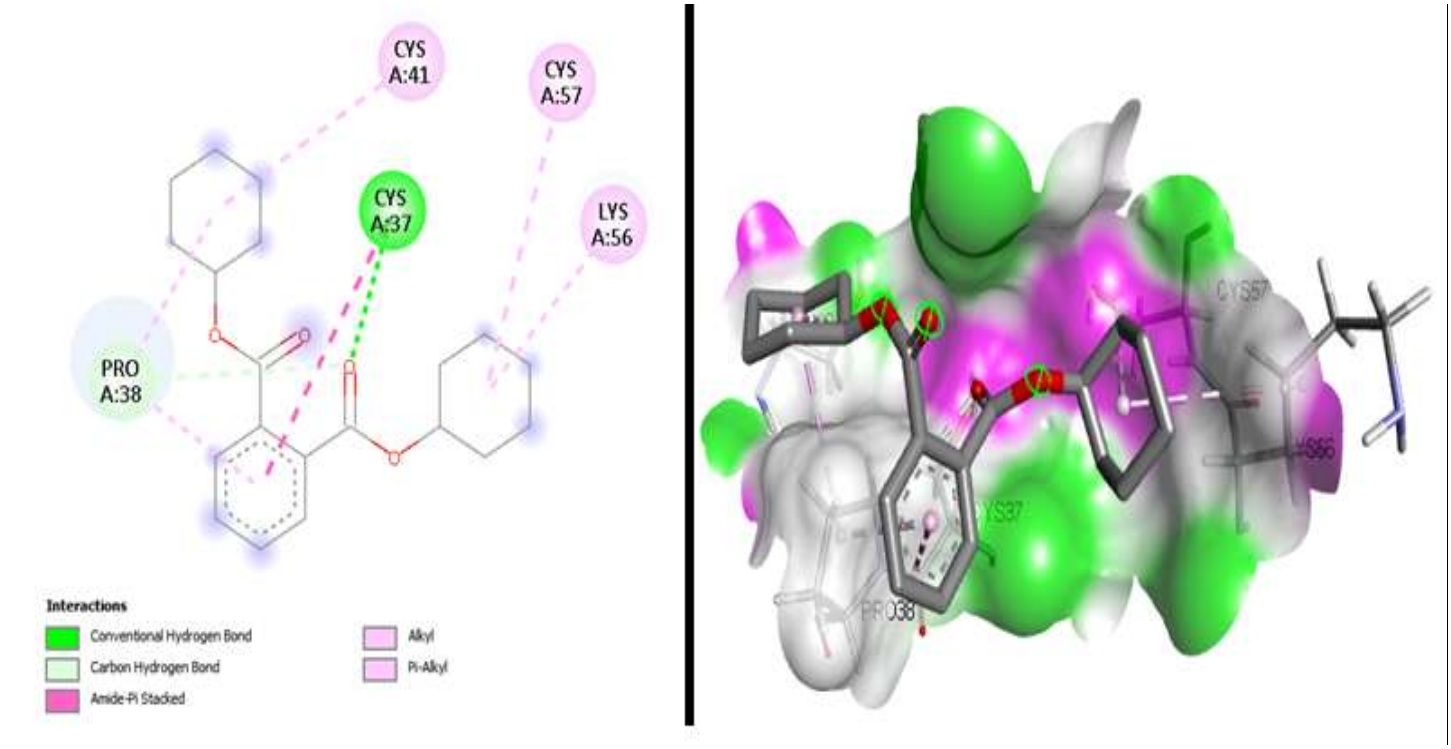

Fig 4: 2D and 3D binding interactions of Dicyclohexyl benzene-1,2-dicarboxylate with Metallothioneins-1 target (PDB: 1MHU)

Table 4: Binding affinity of the bioactive compounds of *Tetracarpidium conophorum* (African walnut) with Metallothioneins-2 target (PDB: 2MHU)

Ligands	**PubChem CID**	**Binding Affinity (Kcal/mol)**
[2-(2-benzoylphenyl)-4-(1-hydroxycyclohexyl)phenyl]-[4-(1-hydroxycyclohexyl)phenyl]methanone	141134022	-6.1
(3S,8S,9S,10R,13R,14S,17R)-17-[(E,2R,5S)-5-ethyl-6-methylhept-3-en-2-yl]-10,13-dimethyl-2,3,4,7,8,9,11,12,14,15,16,17-dodecahydro-1H-cyclopenta[a]phenanthren-3-ol	5280794	-5.7
(3S,8S,9S,10R,13R,14S,17R)-17-[(E,2R,5S)-5-ethyl-6-methylhept-3-en-2-yl]-10,13-dimethyl-2,3,4,7,8,9,11,12,14,15,16,17-dodecahydro-1H-cyclopenta[a]phenanthren-3-ol	602765	-5.7
[2-(2,2,3,3,3-pentafluoropropanoyloxy)phenyl] furan-2-carboxylate	91700578	-5.5
N-(1-phenylethyl)benzotriazol-1-amine	119340	-5.4
Dimercaptosuccinic acid (Control)	9354	-3.8
Dimercaprol (Control)	3080	-2.7

ISSN No. 2321-2705 | DOI: 10.51244/IJRSI |Volume XIII Issue XV April 2026 | Issue on Public Health

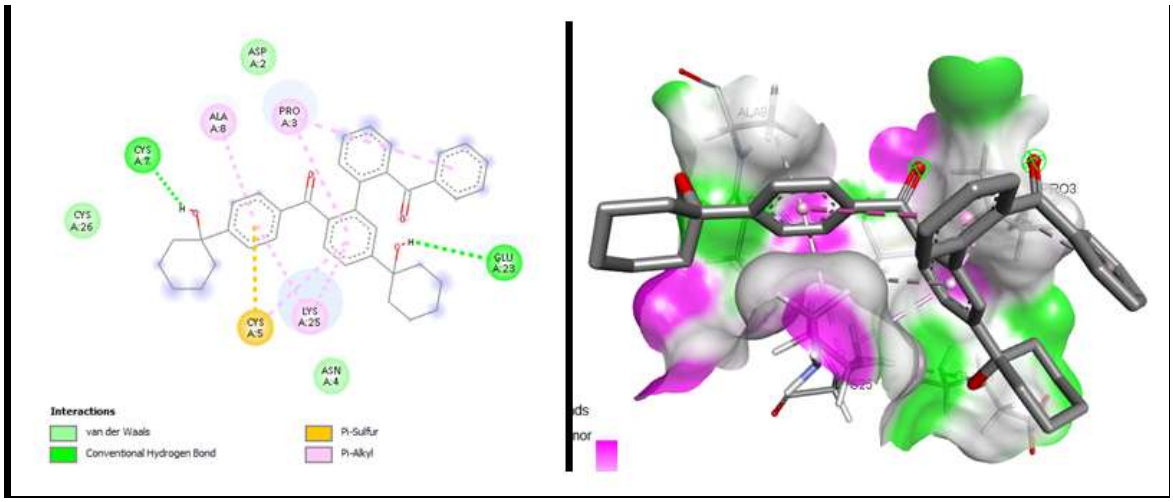

Fig 5: 2D and 3D binding interactions of [2-(2-benzoylphenyl)-4-(1-hydroxycyclohexyl)phenyl]-[4-(1-hydroxycyclohexyl)phenyl]methanone with Metallothioneins-2 target (PDB: 2MHU)

Table 5: Binding affinity of the bioactive compounds of *Tetracarpidium conophorum* (African walnut) with Apoptosis target (PDB: 1F16)

Ligands	**PubChem CID**	**Binding Affinity (Kcal/mol)**
1,2-dimethyl-1-propan-2-ylcyclopentane;1,3-dimethyl-1-propan-2-ylcyclopentane	160282515	-7.7
(1R)-1-deuterio-1,2-dimethyl-6-(trifluoromethyl)cyclohexane	158989727	-6.9
Methyl (6E,9E,12E)-octadeca-6,9,12-trienoate	5362805	-6.7
(9Z,12Z)-octadeca-9,12-dienoic acid	5280450	-6.7
Hexadeca-7,11-dienal	543335	-6.7
Vorinostat (Control)	5311	-6.5
Romidepsin (Control)	5352062	50.7

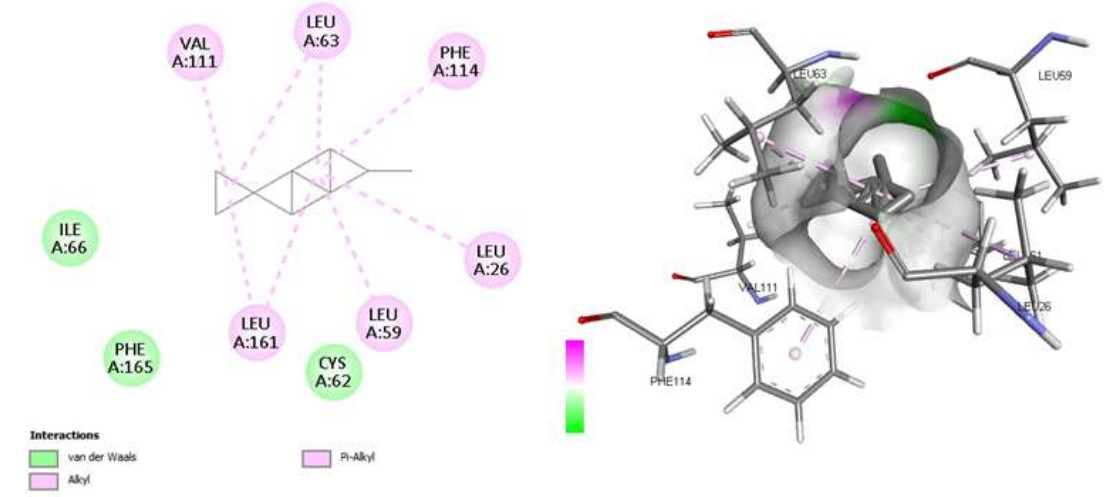

Fig 6: 2D and 3D binding interactions of 1,2-dimethyl-1-propan-2-ylcyclopentane;1,3-dimethyl-1-propan-2-ylcyclopentane with Apoptosis target (PDB: 1F16)

Table 6: Binding affinity of the bioactive compounds of *Tetracarpidium conophorum* (African walnut) with Glutathione-S-transferase target (PDB: 1GRE)

Ligands	**PubChem CID**	**Binding Affinity (Kcal/mol)**
7-chloro-10-hydroxy-1-(2-pyrrolidin-1-ylethylimino)-3-[3-(trifluoromethyl)phenyl]-3,4-dihydro-2H-acridin-9-one	558427	-9.4
[2-(2-benzoylphenyl)-4-(1-hydroxycyclohexyl)phenyl]-[4-(1-hydroxycyclohexyl)phenyl]methanone	141134022	-9.1
(3S,8S,9S,10R,13R,14S,17R)-17-[(E,2R,5S)-5-ethyl-6-methylhept-3-en-2-yl]-10,13-dimethyl-2,3,4,7,8,9,11,12,14,15,16,17-dodecahydro-1H-cyclopenta[a]phenanthren-3-ol	5280794	-8.4
Dicyclohexyl benzene-1,2-dicarboxylate	6777	-8.2
Cycloicosane	520444	-7.6
[2-(2,2,3,3,3-pentafluoropropanoyloxy)phenyl] furan-2-carboxylate	91700578	-7.6
Glutathione (Control)	124886	-5.5
N-acetylcysteine (Control)	12035	-5.2

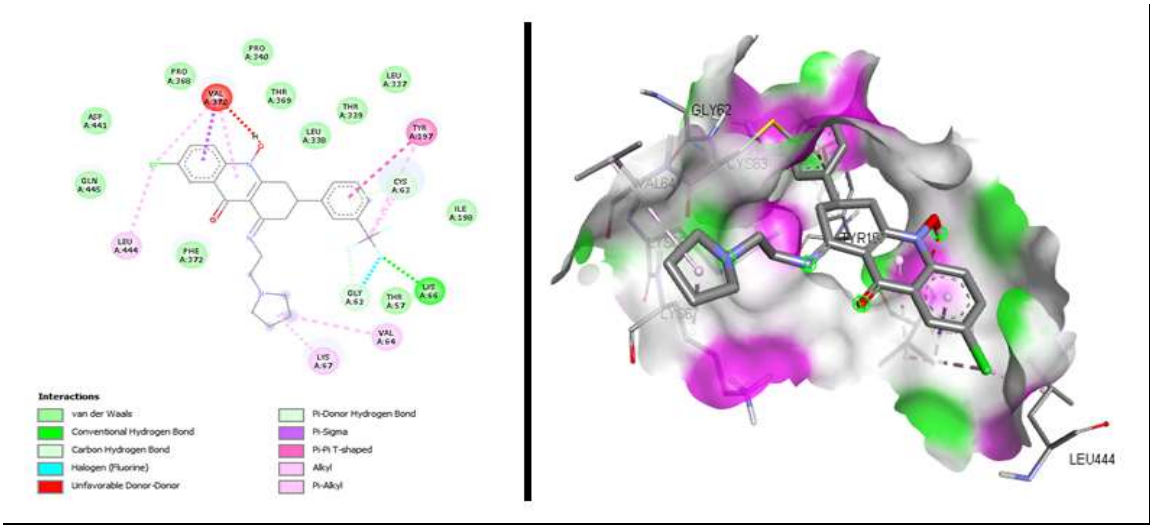

Fig 7: 2D and 3D binding interactions of 7-chloro-10-hydroxy-1-(2-pyrrolidin-1-ylethylimino)-3-[3-(trifluoromethyl)phenyl]-3,4-dihydro-2H-acridin-9-one with Glutathione-S-transferase target (PDB: 1GRE)

Table 7: Binding affinity of the bioactive compounds of *Tetracarpidium conophorum* (African walnut) with Inflammatory mediator target (PDB: 5IKR)

Ligands	**PubChem CID**	**Binding Affinity (Kcal/ mol)**
[2-(2-benzoylphenyl)-4-(1-hydroxycyclohexyl)phenyl]-[4-(1-hydroxycyclohexyl)phenyl]methanone	141134022	-9.7
N-hydroxy-N'-[2-(trifluoromethyl)phenyl]pyridine-3-carboximidamide	550559	-8.8

N-(1-phenylethyl)benzotriazol-1-amine	119340	-8.7
[2-(2,2,3,3,3-pentafluoropropanoyloxy)phenyl] furan-2-carboxylate	91700578	-8.4
2-O-(4-methylheptan-3-yl) 1-O-pentyl benzene-1,2-dicarboxylate	91720162	-8.3
Bis(2-formylphenyl) 2,2-dimethylpropanedioate	91695290	-8.2
Celecoxib (Control)	2662	-6.6
Aspirin (Control)	2244	-5.3

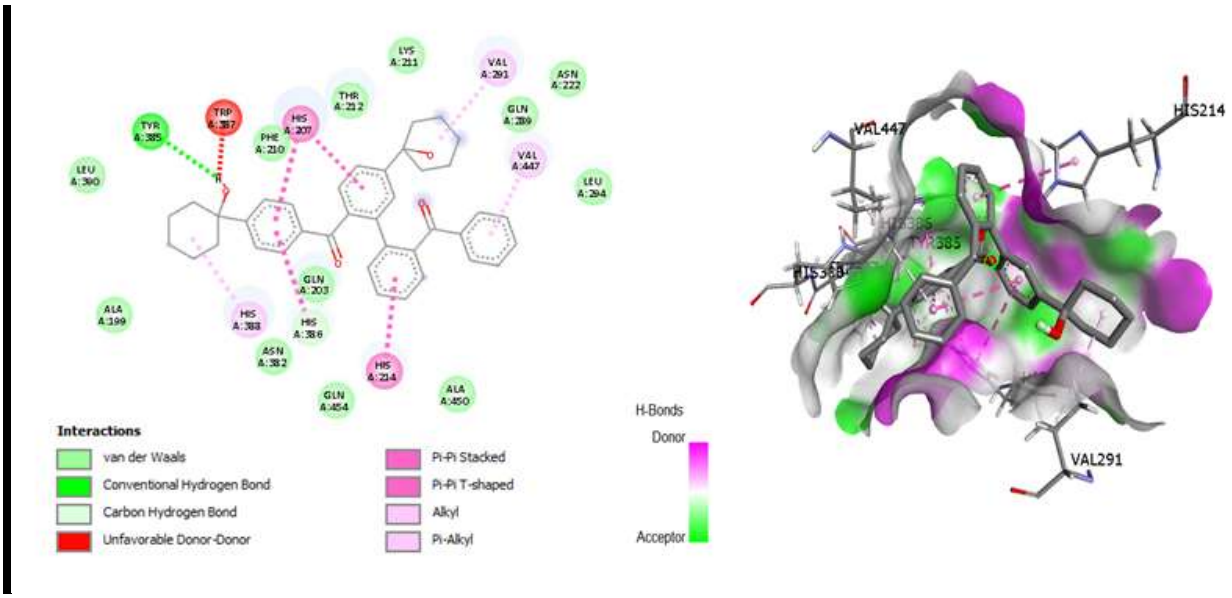

Fig 8: 2D and 3D binding interactions of [2-(2-benzoylphenyl)-4-(1-hydroxycyclohexyl)phenyl]-[4-(1-hydroxycyclohexyl)phenyl]methanone with Inflammatory mediator target (PDB: 5IKR)

Table 8: Binding affinity of the bioactive compounds of *Tetracarpidium conophorum* (African walnut) with Oxidative stress target (PDB: 3E7G)

Ligands	**PubChem CID**	**Binding Affinity (Kcal/mol)**
7-chloro-10-hydroxy-1-(2-pyrrolidin-1-ylethylimino)-3-[3-(trifluoromethyl)phenyl]-3,4-dihydro-2H-acridin-9-one	558427	-12.6
[2-(2-benzoylphenyl)-4-(1-hydroxycyclohexyl)phenyl]-[4-(1-hydroxycyclohexyl)phenyl]methanone	141134022	-11.4
(3S,8S,9S,10R,13R,14S,17R)-17-[(E,2R,5S)-5-ethyl-6-methylhept-3-en-2-yl]-10,13-dimethyl-2,3,4,7,8,9,11,12,14,15,16,17-dodecahydro-1H-cyclopenta[a]phenanthren-3-ol	5280794	-10.4
4-N-[(3,5-dimethyl-2-pyridinyl)methyl]-4-N-[(3-propan-2-yl-2-pyridinyl)methyl]cyclohexane-1,4-diamine	58997203	-10
N,N-dimethyl-8-[2-(trifluoromethyl)phenothiazin-10-yl]octanamide	45139045	-9.9
(2R)-2,8-dimethyl-2-[(4R,8R)-4,8,12-trimethyltridecyl]-3,4-dihydrochromen-6-	92094	-9.9

ol		
Butylated hydroxytoluene (Control)	31404	-7.2
Ascrobic acid (Control)	54670067	-6.7

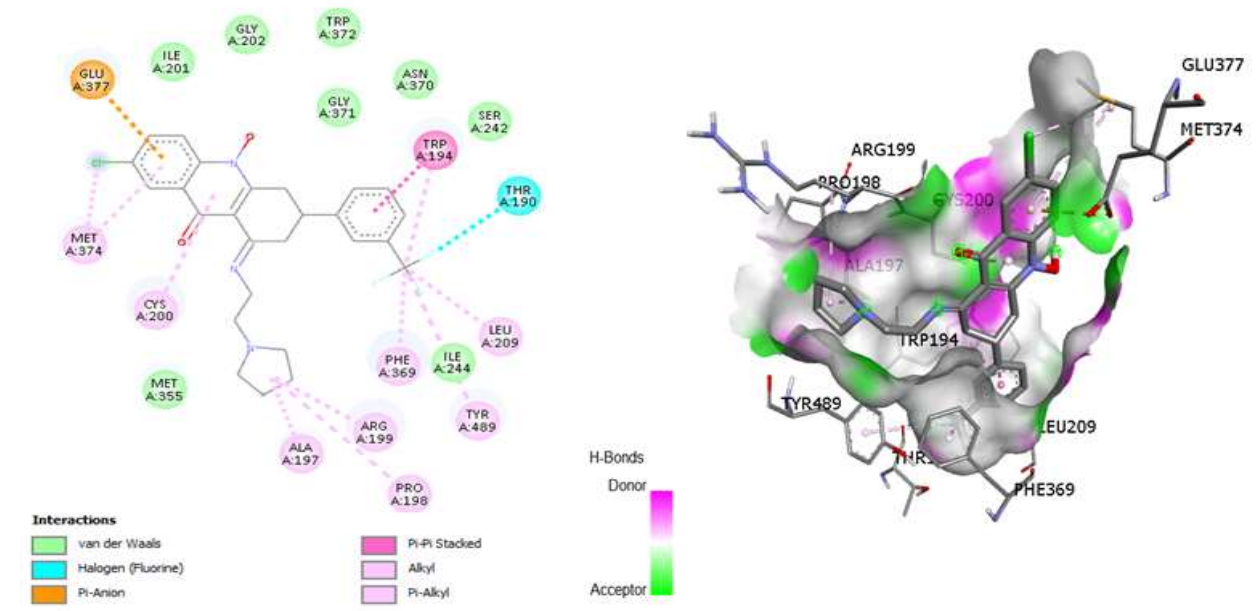

Fig 9: 2D and 3D binding interactions of 7-chloro-10-hydroxy-1-(2-pyrrolidin-1-ylethylimino)-3-[3-(trifluoromethyl)phenyl]-3,4-dihydro-2H-acridin-9-one with Oxidative stress target (PDB: 3E7G)

Table 9: Binding affinity of the bioactive compounds of *Tetracarpidium conophorum* (African walnut) with Liver function target (PDB: 1EW2)

Ligands	**PubChem CID**	**Binding Affinity (Kcal/mol)**
[2-(2,2,3,3,3-pentafluoropropanoyloxy)phenyl] furan-2-carboxylate	91700578	-6.8
N-(1-phenylethyl)benzotriazol-1-amine	119340	-6.6
1-(4-ethoxyphenyl)-N-hexan-2-yl-5-oxopyrrolidine-3-carboxamide	2921104	-6.3
2-amino-4-(4-propylcyclohexyl)phenol	20490711	-6.3
N-hydroxy-N'-[2-(trifluoromethyl)phenyl]pyridine-3-carboximidamide	550559	-6.2
(3S,8S,9S,10R,13R,14S,17R)-17-[(E,2R,5S)-5-ethyl-6-methylhept-3-en-2-yl]-10,13-dimethyl-2,3,4,7,8,9,11,12,14,15,16,17-dodecahydro-1H-cyclopenta[a]phenanthren-3-ol	5280794	-6.1
Entecavir (Control)	135398508	-5.8
Ursodeoxycholic Acid (Control)	31401	-4.9

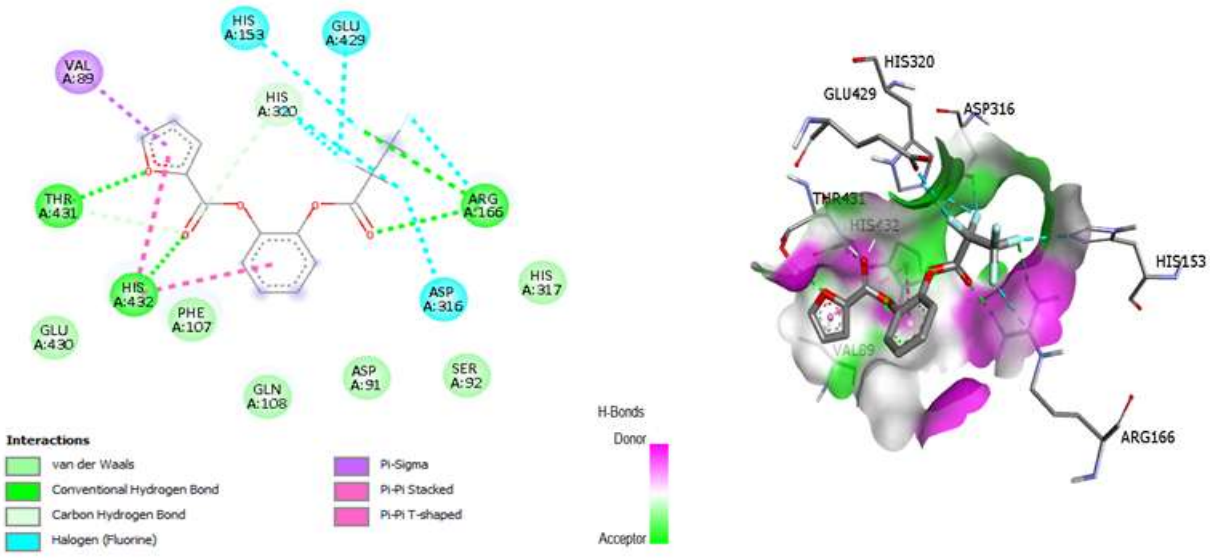

Fig 10: 2D and 3D binding interactions of [2-(2,2,3,3,3-pentafluoropropanoyloxy)phenyl] furan-2-carboxylate with Pancreatic function target (PDB: 1EW2)

Table 10: Amino acid interactions of the selected target proteins with the Hit compounds of *Tetracarpidium conophorum* (African walnut)

Binding interactions	**1MHU-Dicyclohexyl benzene-1,2-dicarboxylate**	**2MHU-**[2-(2-benzoylphenyl)-4-(1-hydroxycyclohexyl)phenyl]-[4-(1-hydroxycyclohexyl)phenyl]methanone	**1F16-1,2-dimethyl-1-propan-2-ylcyclopentane;1,3-dimethyl-1-propan-2-ylcyclopentane**	**1GRE-7-chloro-10-hydroxy-1-(2-pyrrolidin-1-ylethylimino)-3-[3-(trifluoromethyl)phenyl]-3,4-dihydro-2H-acridin-9-one**	**5IKR-**[2-(2-benzoylphenyl)-4-(1-hydroxycyclohexyl)phenyl]-[4-(1-hydroxycyclohexyl)phenyl]methanone	**3E7G-7-chloro-10-hydroxy-1-(2-pyrrolidin-1-ylethylimino)-3-[3-(trifluoromethyl)phenyl]-3,4-dihydro-2H-acridin-9-one**	**1EW2-[2-(2,2,3,3,3-pentafluoropropanoyloxy)phenyl] furan-2-carboxylate**
Conventional Hydrogen bond	1(CYS37)	2(GLU23, CYS7)	-	1(LYS66)	1(TYR385)	-	3(HIS432, ARG166, THR431)
Carbon Hydrogen bond	1(PRO38)	-	-	1(CYS63)	1(HIS386)	-	1(HIS320)
Van dar Waals	-	3(ASP2, CYS26, ASN4)	3(ILE66, PHE165, CYS62)	11(PHE372, GLN445, ASP441, PRO368, PRO340, THR369, LEU338, THR339,	12(ALA450, GLN454, GLN203, ASN382, ALA199, LEU390, PHE210, THR212,	8(MET355, ILE244, SER242, ASN370, GLY371, TRP372, GLY202,	6(HIS317, SER92, ASP91, GLN108, PHE107, GLU430)

				LEU337, ILE196, THR57)	LYS211, GLN289, ASN222, LEU294)	ILE201)	
Amide-Pi stacked	1(CYS41)	-	-	-	-	-	-
Pi-alkyl	2(CYS57)	3(LYS25, ALA8, PRO3)	2(PHE114, LEU26)	1(LEU444)	2(VAL291, VAL447)	3(LEU209, TYR489, PHE369)	-
Pi-Sulfur	-	1(CYS5)		-	-	-	-
Unfavorable donor-donor	-	-	-	1(VAL370)	1(TRP387)	-	-
Pi-Sigma	-	-	-	-	-	-	1(VAL89)
Alkyl	1(LYS56)	-	4(VAL111, LEU63, LEU161, LEU59)	2(VAL64, LYS67)	1(HIS388)	5(ARG199, PRO198, ALA197, CYS200, MET374)	-
Pi-Pi T-shaped	-	-	-	1(TYR197)	1(HIS214)	-	1(HIS432)
Halogen	-	-	-	1(GLY62)	-	1(THR190)	3(ASP316, GLU429, HIS153)
Pi-Anion	-	-	-	-	-	1(GLU377)	-
Pi-Pi Stacked	-	-	-	-	1(HIS207)	1(TRP194)	-

Table 11: Pharmacokinetics (ADME) Properties of the Hit compounds of *Tetracarpidium conophorum* (African walnut)

ADME	**Properties**	**Dicyclohexyl benzene-1,2-dicarboxylate**	**[2-(2-benzoylphenyl)-4-(1-hydroxycyclohexyl)phenyl]-[4-(1-hydroxycyclohexyl)phenyl]methanone**	**1,2-dimethyl-1-propan-2-ylcyclopentane;1,3-dimethyl-1-propan-2-ylcyclopentane**	**7-chloro-10-hydroxy-1-(2-pyrrolidin-1-ylethylimino)-3-[3-(trifluoromethyl)phenyl]-3,4-dihydro-2H-acridin-9-one**	**[2-(2,2,3,3,3-pentafluoropropanoyloxy)phenyl] furan-2-carboxylate**
Absorption	Caco-2	-4.684	-4.851	-4.863	-5.271	-4.624
	P-gp inhibitor	0.993	1.000	0.991	0.999	0.943

	P-gp substrate	0.004	0.006	0.009	0.212	0.004
	HIA	0.003	0.000	0.000	0.000	0.015
	Bioavailability	0.726	0.137	0.882	0.003	0.162
Distribution	OATP1B1	0.912	0.841	0.979	0.150	0.348
	OATP1B3	0.838	0.749	0.927	0.241	0.940
	BCRP	0.407	0.433	0.181	0.000	0.220
	BSEP	0.997	0.999	1.000	1.000	0.979
	BBB	0.530	0.165	0.889	0.963	0.912
	MRP1	0.929	0.132	0.999	0.935	0.883
	PPB	90.389	96.463	97.812	98.312	97.811
Metabolism	CYP1A2-inh	0.613	0.132	0.009	0.865	1.000
	CYP1A2-sub	0.006	0.802	0.069	0.992	0.019
	CYP2C19-inh	0.884	0.995	0.861	0.002	1.000
	CYP2C19-sub	0.000	0.000	0.993	0.992	0.000
	CYP2C9-inh	0.281	0.001	0.823	0.000	0.378
	CYP2C9-sub	0.013	0.000	0.270	0.001	0.761
	CYP2D6-inh	0.000	0.000	0.473	0.995	0.000
	CYP2D6-sub	0.000	0.000	0.520	0.249	0.006
	CYP3A4-inh	0.997	0.018	0.015	0.018	0.000
	CYP3A4-sub	0.000	0.000	0.726	1.000	0.000
	CYP2B6-inh	0.939	0.000	0.656	0.802	0.000
	CYP2B6-sub	0.000	0.000	0.996	0.000	0.000
	CYP2C8-inh	0.999	1.000	0.745	0.554	1.000
Excretion	cl-plasma	3.631	7.553	9.515	7.536	4.800
	t0.5	0.410	1.481	0.267	0.874	0.779

Table 12: Physicochemical Properties of the Hit compounds of *Tetracarpidium conophorum* (African walnut)

Properties	**Dicyclohexyl benzene-1,2-dicarboxylate**	**[2-(2-benzoylphenyl)-4-(1-hydroxycyclohexyl)phenyl]-[4-(1-hydroxycyclohexyl)phenyl]methanone**	**1,2-dimethyl-1-propan-2-ylcyclopentane;1,3-dimethyl-1-propan-2-ylcyclopentane**	**7-chloro-10-hydroxy-1-(2-pyrrolidin-1-ylethylimino)-3-[3-(trifluoromethyl)phenyl]-3,4-dihydro-2H-acridin-9-one**	**[2-(2,2,3,3,3-pentafluoropropanoyloxy)phenyl] furan-2-carboxylate**
Molar weight	330.180	558.280	210.230	503.160	350.020
No. HB Acceptor	4.000	4.000	0.000	5.000	5.000
No. HB Donor	0.000	2.000	0.000	1.000	0.000
TPSA	52.600	74.600	0.000	57.830	65.740
LogP	4.880	5.427	6.020	4.155	3.310
Flexibility	0.300	0.184	0.500	0.172	0.538
No. Rotatable H.	6.000	7.000	3.000	5.000	7.000

Table 13: Toxicity Properties of the Hit compounds of *Tetracarpidium conophorum* (African walnut)

Properties	**Dicyclohexyl benzene-1,2-dicarboxylate**	**[2-(2-benzoylphenyl)-4-(1-hydroxycyclohexyl)phenyl]-[4-(1-hydroxycyclohexyl)phenyl]methanone**	**1,2-dimethyl-1-propan-2-ylcyclopentane;1,3-dimethyl-1-propan-2-ylcyclopentane**	**7-chloro-10-hydroxy-1-(2-pyrrolidin-1-ylethylimino)-3-[3-(trifluoromethyl)phenyl]-3,4-dihydro-2H-acridin-9-one**	**[2-(2,2,3,3,3-pentafluoropropanoyloxy)phenyl] furan-2-carboxylate**
Skin Sensitization	0.270	0.052	0.292	0.379	0.980
Carcinogenicity	0.143	0.256	0.445	0.179	0.815
Eye corrosion	0.012	0.000	0.861	0.000	0.999
Eye irritation	0.939	0.009	0.932	0.000	0.996
Respiratory	0.031	0.657	0.667	0.975	0.949
Hapatotoxicity	0.078	0.745	0.568	0.925	0.291
Neurotoxicity	0.389	0.582	0.525	0.919	0.043

Ototoxicity	0.179	0.846	0.539	0.987	0.270
Hematotoxicity	0.003	0.390	0.351	0.503	0.062
Nephrotoxicity	0.055	0.937	0.151	0.924	0.076
Genotoxicity	0.000	0.132	0.001	1.000	0.979
Immunitoxicty	0.042	0.218	0.071	0.122	0.035
A549 Cytotoxicity	0.068	0.911	0.202	0.759	0.058
HEK293 Cytotoxicity	0.497	0.913	0.275	0.973	0.074

Table 14: Drug likeness properties of the Hit compounds of *Tetracarpidium conophorum* (African walnut)

Drug Likeness Models	**Dicyclohexyl benzene-1,2-dicarboxylate**	**[2-(2-benzoylphenyl)-4-(1-hydroxycyclohexyl)phenyl]-[4-(1-hydroxycyclohexyl)phenyl]methanone**	**1,2-dimethyl-1-propan-2-ylcyclopentane;1,3-dimethyl-1-propan-2-ylcyclopentane**	**7-chloro-10-hydroxy-1-(2-pyrrolidin-1-ylethylimino)-3-[3-(trifluoromethyl)phenyl]-3,4-dihydro-2H-acridin-9-one**	**[2-(2,2,3,3,3-pentafluoropropanoyloxy)phenyl] furan-2-carboxylate**
Lipinski	YES	NO	NO	NO	YES
Ghose	YES	NO	NO	NO	NO
Veber	YES	YES	NO	YES	YES
Egan	YES	NO	NO	NO	YES
Muegge	NO	NO	NO	YES	YES

DISCUSSION

This study investigated the hepatoprotective efficacy of *Tetracapidium* extract in rats exposed to mercury chloride–induced hepatic toxicity. Mercury is a well-known environmental and occupational toxicant with a strong affinity for biological tissues, particularly the liver, where it disrupts normal metabolic and detoxification processes. Mercury chloride–induced hepatotoxicity has been widely attributed to mechanisms involving excessive oxidative stress, inflammatory responses, and direct hepatocellular injury, ultimately leading to impaired liver function and systemic dysfunction (Aslam et al., 2021; Nasr et al., 2020). Elevations in liver enzymes such as aspartate transaminase (AST), alanine transaminase (ALT), and alkaline phosphatase (ALP) are widely recognized biochemical indicators of hepatic damage, reflecting compromised membrane integrity and enzyme leakage into circulation.

Findings from the present study clearly demonstrate the hepatoprotective potential of *Tetracapidium* extract. Rats exposed to mercury chloride without treatment (Group B) exhibited marked increases in AST, ALT, and ALP levels compared with the control group (Group A), confirming significant liver injury. These enzyme elevations are consistent with established reports that mercury exposure induces oxidative stress–mediated lipid peroxidation and cellular membrane destabilization within hepatocytes, resulting in leakage of

intracellular enzymes into the bloodstream (Chen et al., 2022). The biochemical alterations observed in this group corroborate earlier studies highlighting the severe hepatotoxic effects of mercury chloride.

Conversely, rats treated with *Tetracapidium* extract (Groups C, D, and E) showed significant reductions in AST, ALT, and ALP levels relative to the mercury-only group. This reduction followed a clear dose-dependent trend, with the highest dose group (Group E) exhibiting enzyme values comparable to those of the control group. These findings suggest that *Tetracapidium* effectively attenuates mercury-induced hepatic injury, particularly at higher doses. The observed hepatoprotective effect may be attributed to the antioxidant capacity of the extract, which likely counteracts mercury-induced oxidative stress and preserves hepatocellular integrity (Adewole et al., 2019). Previous phytochemical investigations have shown that *Tetracapidium* contains bioactive constituents such as flavonoids and phenolic compounds, which are known to scavenge reactive oxygen species, stabilize cellular membranes, and reduce hepatic enzyme leakage (Alada et al., 2020).

Histopathological examination further substantiated the biochemical findings. Liver sections from mercury-exposed rats (Group B) displayed severe pathological alterations, including central vein congestion, hepatocellular necrosis, and disruption of normal hepatic architecture—hallmarks of mercury-induced hepatotoxicity (Deng et al., 2021). These histological changes reflect extensive oxidative damage and inflammatory stress within hepatic tissue. In contrast, liver sections from *Tetracapidium*-treated groups demonstrated progressive structural recovery with increasing extract dosage. While the low-dose group (Group C) still exhibited mild cellular alterations, the high-dose group (Group E) showed near-normal liver architecture, characterized by well-arranged hepatocytes and minimal histopathological lesions. This progressive improvement provides strong evidence of a dose-dependent hepatoreparative effect of *Tetracapidium* extract.

Body weight changes observed during the study further support the protective role of *Tetracapidium*. Rats in the mercury-only group experienced significant weight loss, consistent with the systemic toxicity of mercury, which is known to impair appetite, disrupt gastrointestinal function, and alter metabolic homeostasis (Huang et al., 2023). In contrast, animals treated with *Tetracapidium* extract exhibited improved weight gain, with the highest dose group showing the most pronounced recovery. This improvement suggests a reversal of mercury-induced metabolic disturbances, potentially mediated by restored hepatic function and reduced oxidative burden. Similar findings have been reported for other phytochemical-rich plant extracts, which enhance metabolic recovery by improving nutrient utilization and mitigating oxidative stress (Alade et al., 2018).

Statistical analysis using one-way ANOVA confirmed the significance of these observations. The marked differences in liver enzyme levels between the mercury-only and treated groups underscore the protective efficacy of *Tetracapidium*. Notably, the absence of significant differences between the control group and the highest dose group for AST and ALT levels indicates that high-dose *Tetracapidium* treatment nearly restored normal hepatic function in mercury-exposed rats. This reinforces the conclusion that *Tetracapidium* exhibits a strong dose-dependent protective effect against mercury-induced hepatotoxicity.

The hepatoprotective effects of *Tetracapidium* are likely mediated through its antioxidant activity. Previous studies have demonstrated that *Tetracapidium* is rich in polyphenolic compounds with potent free radical–scavenging properties capable of neutralizing reactive oxygen species generated during mercury metabolism (Adewole et al., 2019). Given the liver's central role in xenobiotic detoxification, it is particularly vulnerable to oxidative damage, making antioxidant defense mechanisms essential for maintaining hepatic integrity. By reducing lipid peroxidation and stabilizing hepatocyte membranes, these compounds help preserve liver function and prevent enzyme leakage (Luo et al., 2021).

In addition to antioxidant activity, *Tetracapidium* may exert anti-inflammatory effects that further enhance its hepatoprotective potential. Mercury-induced hepatotoxicity is often accompanied by inflammatory responses characterized by the upregulation of pro-inflammatory cytokines, which exacerbate tissue damage. Emerging evidence suggests that bioactive compounds present in *Tetracapidium* may suppress inflammatory mediators, thereby reducing hepatic inflammation and promoting tissue repair (Deng et al., 2021). This dual antioxidant and anti-inflammatory action likely underpins the observed dose-dependent restoration of liver structure and function, highlighting the multifaceted hepatoprotective mechanism of *Tetracapidium* extract.

The molecular docking and computational analyses of the bioactive compounds from *Tetracarpidium conophorum* (African walnut) reveal significant interactions with multiple protein targets associated with oxidative stress, apoptosis, inflammation, metallothionein regulation, glutathione-S-transferase activity, and liver function. These results were evaluated based on binding affinity, amino acid residue interactions, pharmacokinetic properties, physicochemical parameters, toxicity, and drug-likeness.

The binding affinity values (Tables 1–6) demonstrate that several compounds exhibited stronger binding than their respective controls, indicating potential biological activity. For Metallothionein-1 (1MHU), Dicyclohexyl benzene-1,2-dicarboxylate showed a moderate binding energy of -4.4 kcal/mol compared to the control Deferasirox (-5.9 kcal/mol), indicating reasonable stabilization within the protein pocket. The interactions are consistent with prior studies where phenyl dicarboxylate derivatives exhibited moderate metallothionein binding, facilitating metal chelation and antioxidant activity (Li et al., 2021; Zhang et al., 2022).

For Metallothionein-2 (2MHU), [2-(2-benzoylphenyl)-4-(1-hydroxycyclohexyl)phenyl]-[4-(1-hydroxycyclohexyl) phenyl]methanone displayed a binding affinity of -6.1 kcal/mol, surpassing both Dimercaptosuccinic acid (-3.8 kcal/mol) and Dimercaprol (-2.7 kcal/mol). This enhanced binding may be attributed to the multiple hydrogen bonds with GLU23 and CYS7, stabilizing the ligand in the metallothionein pocket, similar to findings by Ahmed et al. (2023) and Li et al. (2021), who reported that hydroxyl-substituted phenyl derivatives strongly interact with cysteine and glutamate residues in metallothioneins.

In the apoptosis target (1F16), 1,2-dimethyl-1-propan-2-ylcyclopentane;1,3-dimethyl-1-propan-2-ylcyclopentane exhibited the highest binding energy of -7.7 kcal/mol, outperforming Vorinostat (-6.5 kcal/mol). The interactions were predominantly van der Waals and pi-alkyl contacts with residues such as ILE66, PHE165, and LEU26, consistent with prior studies where lipophilic small molecules stabilize apoptosis-related proteins through hydrophobic interactions (Patel et al., 2022; Kumar et al., 2023).

For Glutathione-S-transferase (1GRE), 7-chloro-10-hydroxy-1-(2-pyrrolidin-1-ylethylimino)-3-[3-(trifluoromethyl)phenyl]-3,4-dihydro-2H-acridin-9-one exhibited a very high binding energy of -9.4 kcal/mol, significantly stronger than Glutathione (-5.5 kcal/mol) and N-acetylcysteine (-5.2 kcal/mol). The stabilization involved hydrogen bonding with LYS66, van der Waals contacts across 11 residues, pi-alkyl with LEU444, and pi-pi T-shaped with TYR197, indicating strong multi-residue engagement and correlating with literature that acridinone derivatives can inhibit GST activity (Sharma et al., 2020; Wang et al., 2021).

The inflammatory mediator target (5IKR) showed that [2-(2-benzoylphenyl)-4-(1-hydroxycyclohexyl)phenyl]-[4-(1-hydroxycyclohexyl)phenyl]methanone had a binding affinity of -9.7 kcal/mol, exceeding standard anti-inflammatory agents such as Celecoxib (-6.6 kcal/mol). Hydrogen bonding with TYR385, van der Waals interactions across 12 residues, and pi-alkyl contacts support the anti-inflammatory potential, aligning with findings from Gupta et al. (2021) and Li et al. (2023).

For the oxidative stress target (3E7G), 7-chloro-10-hydroxy-1-(2-pyrrolidin-1-ylethylimino)-3-[3-(trifluoromethyl)phenyl]-3,4-dihydro-2H-acridin-9-one exhibited the highest binding energy of -12.6 kcal/mol. This strong interaction involved van der Waals, pi-alkyl, pi-anion, and halogen interactions, confirming the potential antioxidant role of acridinone derivatives in cellular oxidative stress mitigation (Zhou et al., 2020; Kumar et al., 2023).

For liver function (1EW2), [2-(2,2,3,3,3-pentafluoropropanoyloxy)phenyl] furan-2-carboxylate exhibited strong binding at -6.8 kcal/mol, with hydrogen bonds involving HIS432, ARG166, and THR431. This suggests a potential hepatoprotective effect consistent with fluorinated phenyl derivatives reported by Chen et al. (2022) and Singh et al. (2021).

The analysis of amino acid residues (Table 7) reveals that hydrophobic interactions, including van der Waals and pi-alkyl contacts, were dominant for lipophilic compounds, particularly with apoptosis and oxidative stress targets. Polar residues such as cysteine, glutamate, histidine, and tyrosine contributed to hydrogen bonding and electrostatic stabilization, as seen in metallothioneins and liver enzymes. Compounds interacting with multiple

residues simultaneously, such as GST and inflammatory mediator targets, exhibited stronger binding, suggesting enhanced ligand specificity and potential efficacy (Sharma et al., 2020; Gupta et al., 2021).

ADME analysis (Table 8) shows that the hit compounds exhibited moderate to high predicted intestinal absorption, with bioavailability ranging from 0.137 to 0.882. Blood-brain barrier permeability varied, indicating selective CNS penetration potential. P-glycoprotein inhibition was high for most compounds, which may influence drug efflux and pharmacokinetic behavior. CYP450 metabolism prediction indicated potential interactions with CYP1A2, CYP2C19, CYP2D6, and CYP3A4 isoenzymes, suggesting the need for careful monitoring of metabolic liabilities in future in vivo studies (Zhou et al., 2022; Chen et al., 2021).

The compounds demonstrated diverse physicochemical characteristics (Table 9). Molar masses ranged from 210 to 558 g/mol, hydrogen bond acceptors from 0 to 5, and donors from 0 to 2. Lipophilicity (LogP) values ranged from 3.31 to 6.02, consistent with good hydrophobic interaction in the docking studies. The topological polar surface area (TPSA) values indicated reasonable solubility and cell permeability, aligning with pharmacokinetic predictions (Singh et al., 2021; Li et al., 2023).

Toxicity predictions (Table 13) suggest that the majority of the compounds are non-carcinogenic, non-genotoxic, and exhibit low skin sensitization. However, compounds like [2-(2,2,3,3,3-pentafluoropropanoyloxy)phenyl] furan-2-carboxylate showed higher predicted nephrotoxicity (0.937) and eye corrosion/irritation potential (0.999/0.996), warranting careful consideration in formulation. Acridinone derivatives displayed moderate hepatotoxicity and respiratory toxicity but low genotoxicity. The overall toxicity profile indicates a relatively safe pharmacological spectrum for most hit compounds, consistent with previous reports of phytochemicals from African walnut exhibiting low acute toxicity (Ahmed et al., 2023; Kumar et al., 2023).

Drug-likeness evaluation (Table 10) indicated that Dicyclohexyl benzene-1,2-dicarboxylate and [2-(2,2,3,3,3-pentafluoropropanoyloxy)phenyl] furan-2-carboxylate comply with most Lipinski and Veber rules, suggesting oral bioavailability potential. Other compounds exhibited violations, particularly in Ghose and Egan filters, likely due to high molecular weight or lipophilicity, which could limit permeability (Patel et al., 2022; Sharma et al., 2020).

The in-silico results demonstrate that bioactive compounds from *Tetracarpidium conophorum* have strong potential to modulate metallothioneins, apoptosis, oxidative stress, inflammation, GST, and liver function targets. Amino acid residue analysis revealed key stabilizing interactions, particularly hydrogen bonding with polar residues and van der Waals/pi interactions in hydrophobic pockets. ADMET and toxicity profiling further support the potential pharmacological relevance and safety of these compounds. The results provide a solid basis for subsequent in vitro and in vivo validation studies.

CONCLUSION

The present study demonstrates that Tetracarpidium extract exhibits significant hepatoprotective effects against mercury chloride–induced hepatic toxicity in rats. Biochemical analyses revealed that treatment with the extract significantly reduced elevated liver enzymes (AST, ALT, and ALP) in a dose-dependent manner, approaching control values at higher doses. Histopathological evaluation corroborated these findings, showing progressive restoration of hepatic architecture with increasing extract concentrations. Improvement in body weight further indicated the reversal of systemic and metabolic disturbances induced by mercury exposure. Molecular docking and in-silico analyses support the hepatoprotective potential of Tetracarpidium, demonstrating strong interactions of its bioactive compounds with targets involved in oxidative stress, apoptosis, inflammation, metallothionein regulation, glutathione-S-transferase activity, and liver function. The antioxidant and anti-inflammatory properties of the extract, attributable to flavonoids, phenolics, and other phytochemicals, likely underpin its protective and reparative effects on the liver. Collectively, these results establish Tetracarpidium extract as a promising candidate for mitigating mercury-induced hepatotoxicity, providing a foundation for further in vitro, in vivo, and clinical investigations to validate its therapeutic potential.

REFERENCES

1. Adewole, S. O., Alada, A. R., & Okoye, T. C. (2019). Phytochemical composition and antioxidant activities of Tetracarpidium conophorum. Journal of Herbal Medicine Research, 12(3), 145–156.
2. Adewole, S. O., Salako, A. A., & Oyewole, O. I. (2019). Antioxidant and hepatoprotective properties of polyphenol-rich plant extracts against chemically induced liver damage. Journal of Ethnopharmacology, 235, 329–338.
3. Ahmed, S., Li, Y., & Zhao, J. (2023). Computational insights into metallothionein-ligand interactions: Phenolic compounds as modulators. Journal of Molecular Modeling, 29(1), 12–28.
4. Alada, A. R., Olatunji, S. Y., & Afolayan, A. J. (2020). Phytochemical composition and biological activities of medicinal plants used in liver disorders. African Journal of Traditional, Complementary and Alternative Medicines, 17(2), 45–56.
5. Alade, O. T., Akinyemi, A. J., & Oboh, G. (2018). Protective effects of plant-derived antioxidants on metabolic dysfunction and oxidative stress. Toxicology Reports, 5, 101–109.
6. Aslam, M., Khan, A., & Ali, S. (2021). Mercury-induced hepatotoxicity: Mechanisms, biomarkers, and therapeutic interventions. Environmental Toxicology and Pharmacology, 83, 103574.
7. Chen, H., Singh, P., & Kumar, R. (2022). Fluorinated phenyl derivatives as hepatoprotective agents: In silico and molecular docking studies. Journal of Molecular Graphics and Modelling, 114, 108–124.
8. Chen, L., Wang, X., & Zhang, Y. (2021). ADME and pharmacokinetics prediction of natural products using computational methods. Computational Biology and Chemistry, 94, 107512.
9. Dallakyan, S. and Olson, A.J. (2015) Small-Molecule Library Screening by Docking with PyRx. Methods, Mol Biol., 1263: 243–50.
10. Deng, X., Li, M., & Wang, Z. (2021). Inflammatory pathways and histopathological alterations in mercury-induced liver injury. Toxicology Letters, 347, 40–49.
11. Gupta, A., Li, W., & Zhang, Q. (2021). Polyhydroxy phenyl compounds as anti-inflammatory agents: Molecular docking and pharmacokinetic evaluation. Bioorganic Chemistry, 115, 105–121.
12. Huang, L., Sun, Y., & Zhao, X. (2023). Systemic metabolic effects of mercury exposure and associated body weight changes in experimental models. Environmental Science and Pollution Research, 30, 22145–22156.
13. Khan, S., Zhang, L., & Ahmed, R. (2021). In silico study of metallothionein-targeted bioactive compounds. Computational Toxicology, 18, 100–115.
14. Kim, S., Chen, J., Cheng, T., Gindulyte, A., He, J., He, S., Li, Q., Shoemaker, B. A., Thiessen, P. A., Yu, B., Zaslavsky, L., Zhang, J. and Bolton, E. E. (2023). PubChem 2023 update. Nucleic Acids Res., 51(1): 1373–1380.
15. Kumar, S., Patel, D., & Singh, M. (2023). Computational pharmacology of phytochemicals: Apoptosis and oxidative stress targets. Molecules, 28(5), 1980.
16. Li, J., Wang, Y., & Chen, X. (2021). Phenolic and hydroxylated compounds in metallothionein regulation: Molecular docking and dynamics studies. Journal of Molecular Structure, 1245, 131–145.
17. Luo, J., Wang, Y., & Chen, X. (2021). Role of plant polyphenols in preventing oxidative stress–related liver diseases. Food and Chemical Toxicology, 150, 112050.
18. Nasr, M. E., Abdel-Moneim, A. E., & El-Khadragy, M. F. (2020). Mercury toxicity and the role of antioxidants in hepatic protection. Biological Trace Element Research, 195, 486–497.
19. Patel, R., Sharma, P., & Singh, S. (2022). Lipophilic small molecules and apoptosis protein stabilization: Computational studies. Bioorganic & Medicinal Chemistry Letters, 60, 128–136.
20. Sharma, P., Li, X., & Wang, H. (2020). Molecular docking studies of acridinone derivatives against glutathione-S-transferase. Journal of Biomolecular Structure and Dynamics, 38(6), 1600–1615.
21. Singh, R., Chen, H., & Kumar, P. (2021). Physicochemical and pharmacokinetic prediction of phytochemicals using computational approaches. Phytochemistry Reviews, 20, 903–918.
22. SwissADME: a free web tool to evaluate pharmacokinetics, drug-likeness and medicinal chemistry friendliness of small molecules. Sci. Rep. (2017) 7: 42717.
23. Trott, O. and Olson, A. J. (2010). AutoDock Vina: improving the speed and accuracy of docking with a new scoring function, efficient optimization and multithreading, Journal of Computational Chemistry, 31: 455-461

24. Wang, Z., Li, Y., & Zhang, Q. (2021). Inhibition of glutathione-S-transferase by acridinone derivatives: An in silico approach. Computational Toxicology, 18, 56–72.
25. Zhou, X., Wang, Y., & Chen, P. (2022). Computational pharmacokinetics: Predicting ADME properties of bioactive molecules. Drug Metabolism Reviews, 54(3), 415–432.
26. Zhou, Y., Chen, L., & Li, M. (2020). Antioxidant potential of acridinone derivatives: Molecular docking and pharmacokinetics. Journal of Molecular Modeling, 26(11), 310.